International Journal of Nanoelectronics and Materials
Volume 16, No. 4, October 2023 [891-904]

Preparation and characterization of Au quantum dots using laser in benzene and study of the pulse Energy effect on quantum size

Luma Talib[1*], Abdulrahman K Ali[1], Alaa Ghani Hussein[2]

[1]Applied Sciences Department, University of Technology, Baghdad, Iraq
[2]Department of Pathology Al-Nahrain University/College of Medicine

Received 13 October 2022, Revised 5 January 2023, Accepted 8 March 2023

ABSTRACT

Here, findings from a study on pulsed laser ablating of noble Au targets submerged in benzene solvent and a study on the effect of pulse energy on quantum size are presented. Three samples of gold quantum dots (AuQDs) are synthesized at pulse fluence of 4, 8, and 12 J/cm^2, which is referred to as F1, F2, and F3, respectively. The prepared AuQDs were characterized by UV-Vis, HR-TEM, XRD, XPS, EDX, FTIR, Raman spectroscopy and Photoluminescence measurement. AuQDs that were synthesized have monocrystalline and cubic (FCC) structure, according to XRD patterns. It was found that the direct optical energy gap of AuQDs is enhanced to 2.6 eV. The emission peak of AuQDs photoluminescence emission spectra is at roughly 481, 445, and 437 nm, for F1, F2, F3 samples, respectively. The quantum size was reduced to 2 nm for sample F3. This strategy has the ability to prepare pure AuQDs in one step, with promising biosensor and bioimaging applications.

Keywords: gold, Quantum dots, Laser ablation, Benzene.

1. INTRODUCTION

AuQDs are more attractive and particularly investigated due to their noble characteristic, ultrafine size, low toxicity, good biocompatibility and long-term stability. Considering these features, several studies have been conducted on their application in the fields of biomedical biosensing, bioimaging, antibacterial, anticancer, solar cells; light-emitting diodes [1]. Quantum dots are often referred to as fluorescent semiconductor nanocrystals [2]. Their extremely small size (less than 10 nm) renders their optical and electronic properties different from those of bulk materials [3]. QDs have a desirable fluorescence spectrum, which makes them the ideal fluorophores for biological applications. Bio-conjugated QDs represent the worthiest prospects for a wide range of data and graphic kinds of technology, they are investigated as instruments for the location of gene and drug development [4]. The type of synthesizing used can have a significant impact on the QDs' characteristics. The synthesizing of such nanomaterials could be divided into two categories: top-down and bottom-up preparation techniques. Top-down techniques include laser ablating, electrochemical etching, liquid-phase exfoliating, electron beam lithography, and other techniques for directly cleaving bulk materials into nanoscale QDs. Bottom-up techniques involve the transformation of QDs from acceptable molecular precursors under certain circumstances such as hydrothermal/solvothermal, microwave irradiation, soft-templating, pyrolysis, and wet chemical processes [3]. Laser ablating represents a technique for producing nanoparticles such as semiconductor QDs [5, 6], metal nanoparticles [7], and core-shell nanoparticles [8, 9]. This technique is a revolutionary synthesizing strategy that uses fewer chemicals and a simple synthetic process to manufacture clean electrocatalysts with no contaminants that have active sites [3].

* Corresponding author: luma.talib93@gmail.com

Ablating efficiency and features of produced particles are strongly influenced by a number of elements, for instance the laser's wavelength that impinging the objective, the effective liquid medium, the ablation time duration, the laser power and the presence or the absence of surfactants [8,9]. The average particle size decreases with increasing ablating laser pulse power [10]. Increased laser power obviously increases the temperature of the ablated material and a faster quenching rate may be involved, which causes the reduction of the sizes of the nanoparticles. The size of particles also becomes more uniform with increasing ablating laser pulse power [11]. The nanoparticle formation is dependent on the absorption efficiency. The absorption of laser light causes the fragmentation of particles [12]. There are no detailed previous studies on the use of laser in preparing gold quantum dots, only one study prepared gold in aromatic solvents without studying the effect of laser parameters on quantum size [13].

In this work, we describe an approach for studying the impact of changing laser pulse energy upon the quantum for preparing ultra-small and pure AuQDs in benzene. Moreover, analyze the structural, morphological, and optical characteristics of the AuQDs using UV-VIS, XPS, EDX, XRD, FTIR, Raman shift, analysis, and HR-TEM. Engineers and scientists can now produce pure AuQDs in a single step using our discoveries to improve certain optic or electric qualities for particular usages.

2. EXPERIMENTAL PART

Preparing AuQDs was done by abrading a pure gold plate (99.999% pureness) that had been put in a beaker with 2 ml of benzene using a pulsed Nd:YAG laser. Whereas the Nd-YAG laser was utilized, it had a wavelength of 1064 nm, at a laser fluence of 4, 8 and 12 J/cm^2, which denoted F1, F2 and F3, respectively. The ablation process took around 25 minutes. AuQDs were successfully dissolved into a colloidal solution, which was clearly demonstrated by the solution transformation from transparent white to golden yellow. When compared to PLAL techniques, traditional wet-chemical methods for preparing colloidal nanoparticles and nanocomposite materials have a number of disadvantages. Figure 1 shows the experimental setup for laser ablating for the objective immersed within benzene.

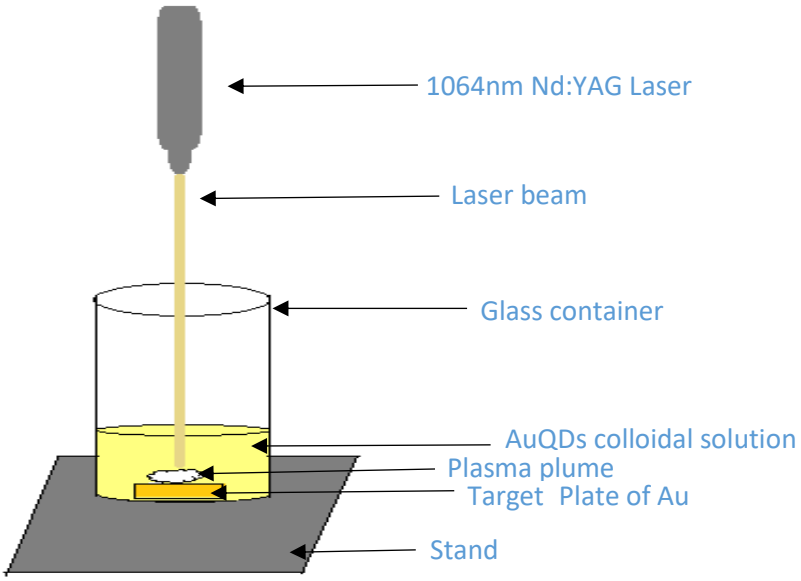

Figure 1. Experimental setup for laser ablating for the AuQDs.

3. CHARACTERIZATION

The UV/VIS spectra were collected utilizing a Perkin Elmer Lambda 365 UV/VIS spectrometer. The FluroMate FS-2 Spectrometer's PL Lamp System was used to capture the photoluminescence (PL). The X-ray photoelectron spectroscopy (XPS) information was acquired by utilizing the K-alpha X-ray photoelectron spectrometer (UK-made Thermos Fisher Scientific kind). The X-ray diffracting (XRD) device was [XRD-6000, SHIMADZU, JAPAN, 220 V/50 Hz] spectrometer, while EDX (Energetic Dispersing X-Ray Spectroscopy) was Bruker Company/ GermanyXFlash_6l10/Model. Fourier transform infrared (FT-IR) analysis was performed (using Perkin Elmer). The JEOL model JEM 2100F was used for a high-resolution transmitting electronic microscopy (HR-TEM), and Raman was collected using a device with a preset 532 nm Raman spectrometer.

4. RESULTS AND DISCUSSION

X-ray diffracting (XRD) represents an extensively utilized analytic method to analyze molecules and crystalized kinds of structure; it measures the particle sizes and degree of crystallinity. The X-ray diffracting pattern of AuQDs is produced by laser ablation in benzene (F3) and deposited on glass substrate by drop casting, as shown in Figure 2, where Au quantums have cubic (fcc) crystal structure with three main peaks located at 38.18°, 44.25°, 64.55° ,77.5° corresponding to the (111), (200), (220), (311) planes, respectively, this was confirmed by comparison with JCPDS Card No. 04-0783 [8]. Due to its greater band gap, the fcc structure represents the most intriguing one. The fcc constructed at F3 displays a band gap of 2.6 eV (in Figure 6b), this is significantly wider than the 1.5 eV energetic gap of the identically sized bcc-constructed Au_{38} (gold nanoparticles have 38 gold atoms) [9].

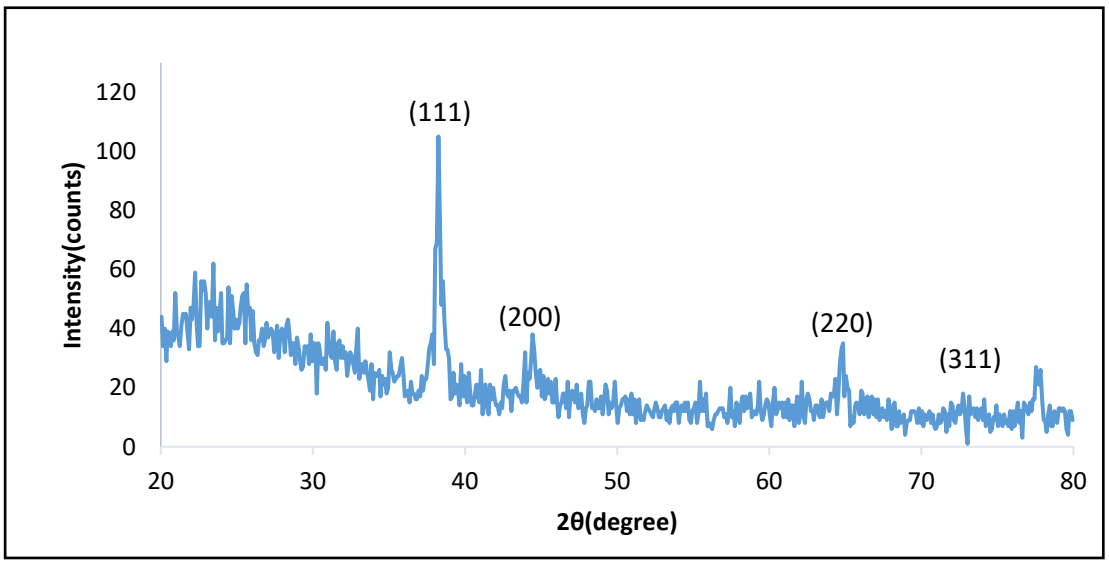

Figure 2. XRD analysis of F3 AuQDs samples.

The energetic dispersing X-ray (EDX) analysis of the AuQDs further established the gold metals' existence, see (Figure 3). The normal counts of the elements obtained were, Si=51.29, C=21.34, Au=23.25, Sb=2.62, Ca=1.50. The EDX spectrum of AuQDs demonstrates the distinct presence of Au peaks at 2.1 KeV, which is the typical absorption peak of the AuQDs. The Si peak at 1.75 KeV can be also found due to the presence of the silicon wafer, which was used as a support for Au. Strong noise signals, including Ca, C, and Sb, were shown by carbon signals, which are caused by

the surfactant. This may be due to the presence of impurities in benzene, benzene vaporization or the interaction of colloidal solvent with the glass chip that the thin film was deposited on it [14,15]. Figure 3b shows the images of mapping results that explain the percentage of elements contained in the sample.

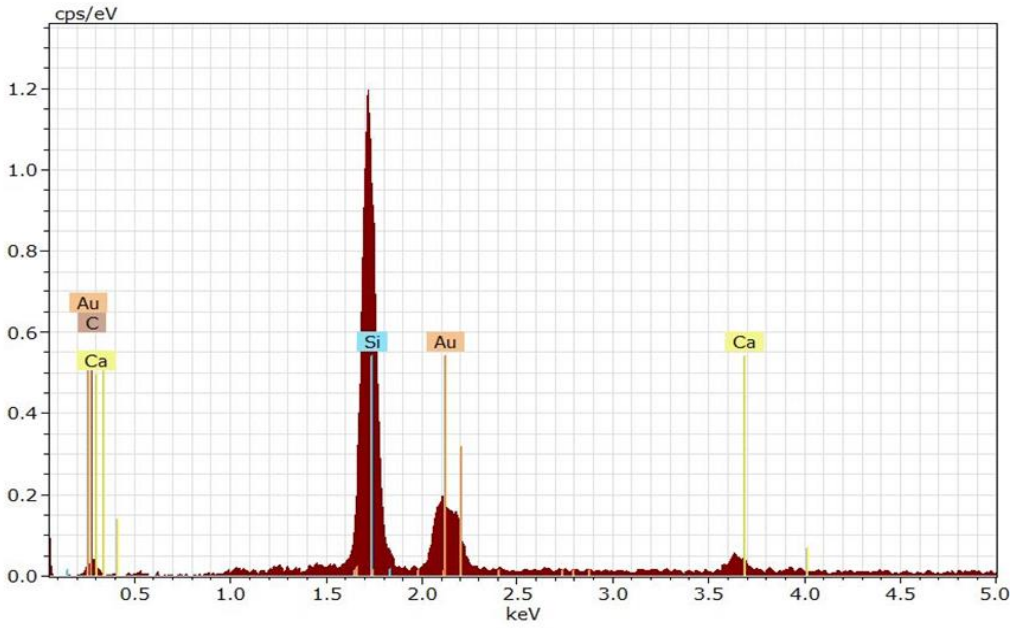

Figure 3a. Energy dispersive X-Ray analysis for F3 AuQDs.

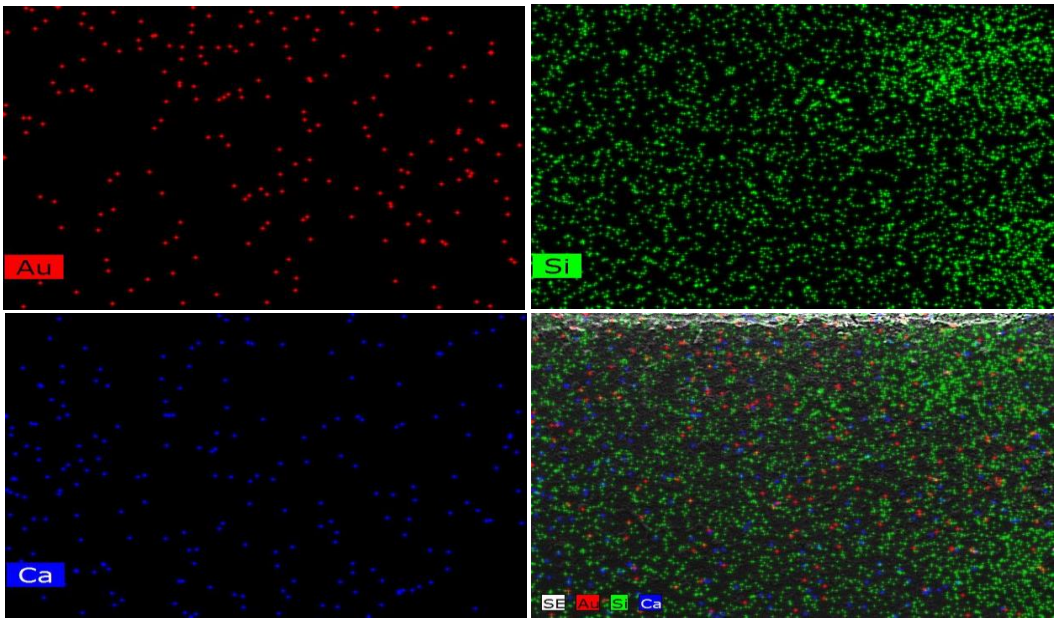

Figure 3b. Images of mapping of F3 AuQDs sample.

Fragmentation could only happen when nanoparticles come into direct contact with the white lighting supercontinuum. The super continuum's white lighting is absorbed by nanoparticles, which then fragment in accordance with the Coulomb explosion method and re-nucleate into Nano clusters that exist within the surrounding fluid. Under such a regime, the fragmentation can be defined by tiny nanoparticle sizes of (10 nm) and poor size dispersing. Contrary to conventional wisdom, the solvent is exposed to laser radiation throughout the experiment cuvette, resulting in homogenous conditions for quantum dots to fragment in a broad volume region and provide a "fine" fragment regime. The importance of the optic breakdown for solid

target geometry grows as the pulse energy rises. The surfaces' melting and hardening of the nanoparticles trapped in plasma is an option. Additionally, we could not rule out the possibility that a second thermal process of nanoparticle evaporation is at play, which may be the cause of the shrinkage of nanoparticle size at high laser energy [16]. The nanoparticles at great energy exhibited a consistent spherical form, as seen in HR-TEM. However, when the pulse energy increased, the size of the nanoparticles shrank to 10 nm. In this instance, contrary to cases with little energy, the nanoparticles exhibited irregular shapes and got connected by filament, pointing to the possibility of thermic alteration of the nanoparticles [11,13]. The HR-TEM study verified the existence of metal particles with a QDs size. The particles had a diameter of less than 10 nm and exhibited a spherical form. The HR-TEM images in Figures (4-a, b,c), (4-d,e,f), (4-g,h,i) demonstrated the production of quantum particles that are spheres and monodispersed, and these images explain the influence laser fluence F1, F2 and F3, respectively, the images refer to the AuQDs results at magnifications (20,10,5) nm from left to right, respectively. The surfaces of Fcc- constructured metal_Nano crystals have a propensity to twin particles with the lowest energy faces around them (111) [17]. By concentrating the beam of electrons on a gold bar nanocluster, the chosen region electron diffracting patterns were obtained to verify the AuQDs' crystalline character. According to the line profile brightness of the corresponding HR-TEM picture, the crystalline lattice space (d-space) is 0.22 nm (fig.4-k). The tiny electron diffraction (Fig. 4-l) showed that the fcc single-crystal AuQDs contained via the 111 crystalline basal plane may be identified by the seven brilliant spots with a hexagonal shape [18]. The (1 1 1), (2 0 0), (2 2 0), and (3 1 1) planes were identified by the independent reflecting characteristic of the brilliant circular structure of the wide-angle electron diffracting pattern. Figure (4n,o,p) shows the particle size distributing within the ranging of 1-9 nm and average sizing of 5, 3.5 and 2 nm for F1, F2 and F3 AuQDs samples, respectively. According to this outcome, the QDs were primarily single-crystal QDs. The findings of the XRD investigation conducted for this study were well matched by the HR-TEM analysis of the AuQDs' manufacturing results. The charging carriers within such clusters became quantized and the valence plus conduction bands were divided into quantifiable and particular electronic states as a result of the proven ultra-small size [19].

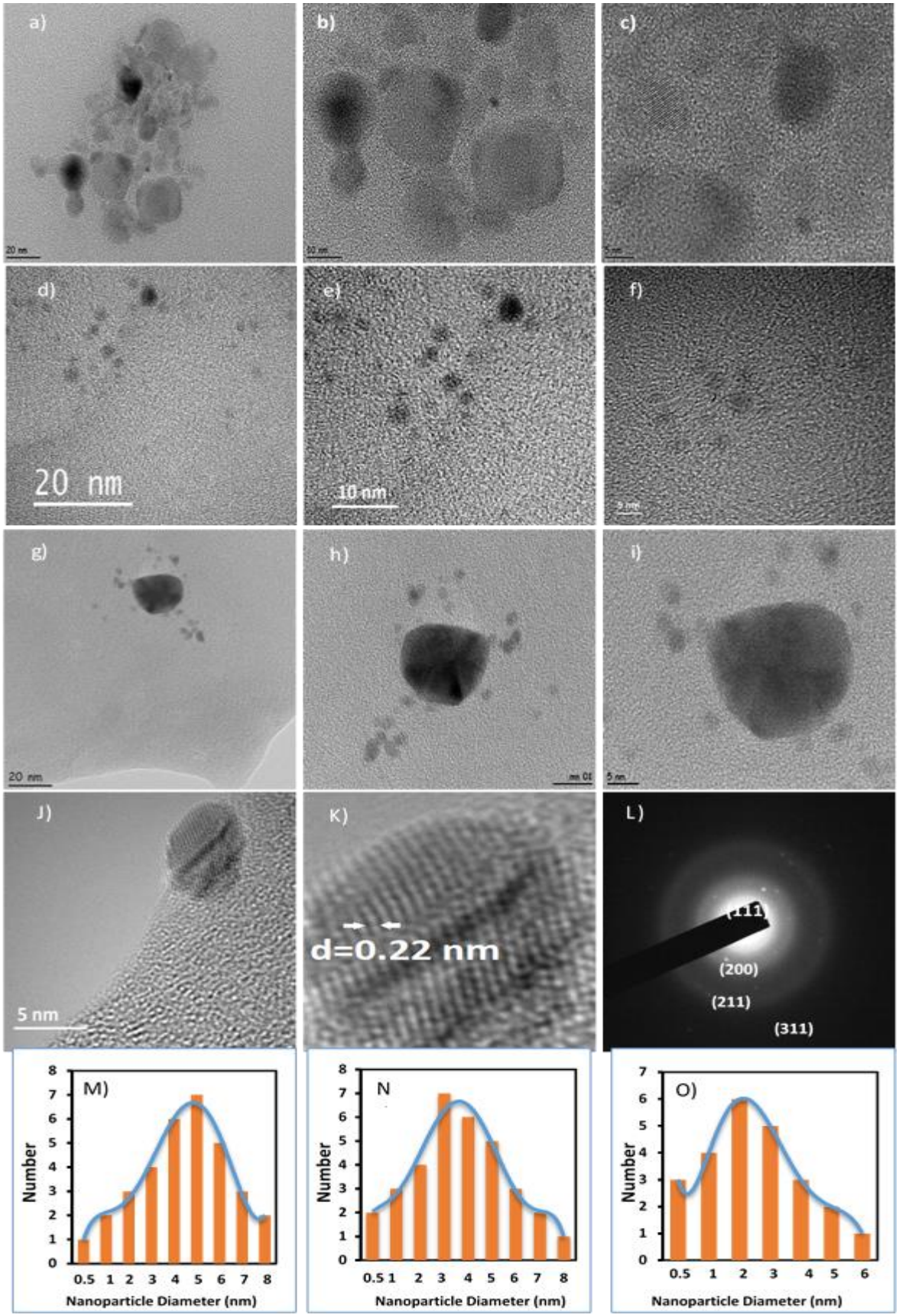

Figure 4. HR-TEM of AuQDs F1 (a-c), F2 (d-f) and F3 (g-i) at magnification of (20, 10, 5 nm) from left to right, respectively; the selected area electron diffraction (SAED) pattern of F1 AuQDs (j); the crystal lattice spacing (d-spacing) (k); the wide-angle electron diffraction pattern (l); and the quantum size distribution of F1 (m), F2 (n) and F3 (o), respectively.

AuQDs is present in F3, which is demonstrated by the XPS surveying spectra (Figure 5a). The image also displays several peak characteristics of various components, among the most intensive being C 1s (285.08 eV) as well as oxygen O 1s. These peak characteristics are along with numerous gold bind energies (i.e., Au4f, Au4d, Au4p, and Au4s) (532.08 eV). The existence of graphite was demonstrated by the high C 1s peak that was focused at 285.08 eV. A single carbon signal at 285.08 eV was visible in the XPS examination, which supported the production of graphite [20]. The amorphous carbon also restricted particles' growth. The graphite forming could be clarified by requesting the graphitic carbon preparations depending upon the pyrolysis of aromatic solvents such as benzene, this was reported in preceding research [21]. The laser's preparation of AuQDs was confirmed by the sharp, intensive bind energy peak at 89.18 eV, linked to Au 4f5/2, and the weaker peak at 83.88 eV, linked to Au 4f7/2 (fig. 5b). According to our findings, the pre-made clusters feature QDs properties with an Au+ oxidizing state. This demonstrated the success of the laser-assisted production of steady and pure AuQDs [22]. Due to the smaller size of these gold nanoclusters, a greater bind energy peak was seen for F3, this was explained by their higher binding energy. This is consistent with the observation that when quantum size decreases, gold's binding energy increases [23]. Furthermore, the electron donation from the Au center atoms to the thiolates existing on the QDs surface might be attributed to the modest bind shifts of the 4f5/2 as well as the 4f7/2 bind energies of AuQDs [24].

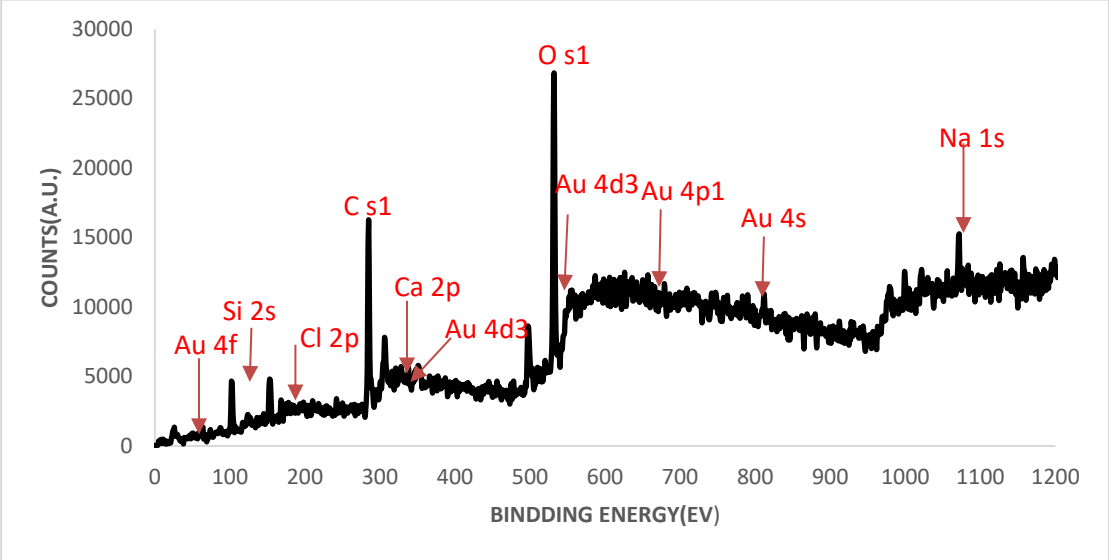

Figure 5a. XPS scan spectrum of F3 AuQDs samples.

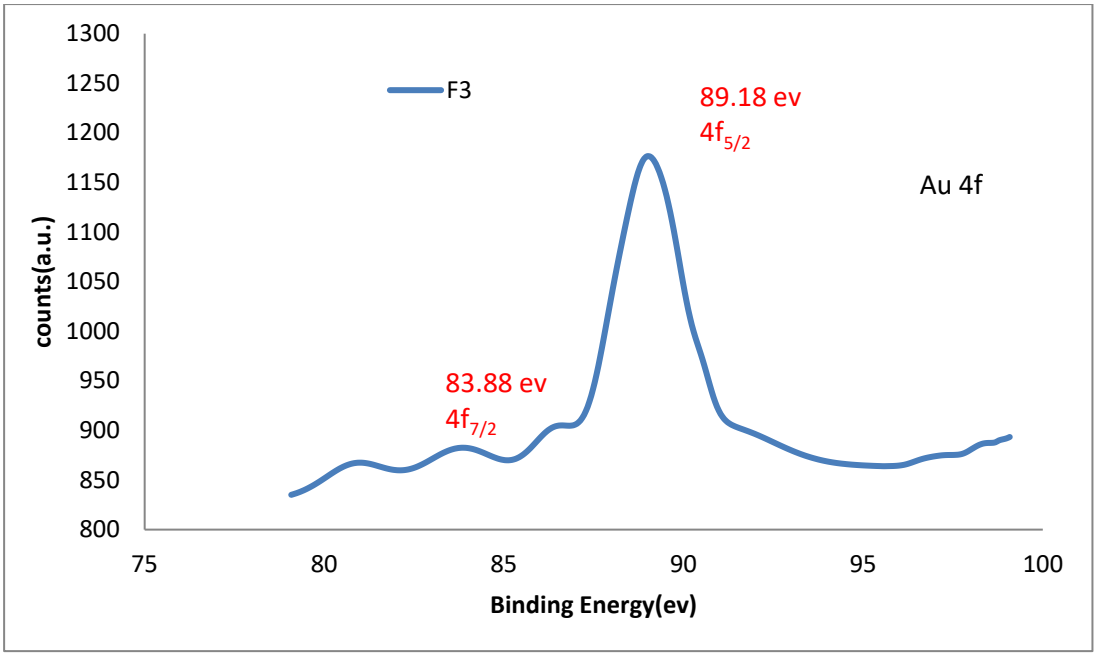

Figure 5b. XPS spectrum of F3 AuQDs.

UV-Vis analysis was conducted to carry out the AuQDs' initial characterization. Figure 6a illustrates the UV-Vis spectra of the colloidal AuQD samples F1, F2, and F3, each of which has an absorbing band with maximum values at 310, 311 and 313 nm, respectively. This is an absorbing characteristic of metallic AuQDs caused by the surficial Plasmon resonant (SPR), suggesting the existence of an Au Quantum dot in the solvent [25, 26]. The formation of nanoparticles shifts the SPR band to blue, spherical nanoparticles and the uniform dispersion of created Nanoparticles [27]. According to a previous study [28], such absorbing maxima are associated with spherical (or almost spherical) AuQDs. HR-TEM images and the accompanying statistical and morphological analysis were used to confirm such findings. Figure (6b) demonstrates that the estimated energy band gaps (Eg) for F1, F2, and F3 AuQDs at the different laser energies used were 2.35, 2.5, and 2.6 eV, respectively. This result agrees with the analysis that because of the intra-band excitation of the conducting electron by photons, the optical absorption of metal nanoparticles may mechanically explain the quantum [29]. Some conduction electrons are held by particular atoms in Qds, while others are unrestricted and move among atoms to create metal kinds of bond that glues the metallic nanoparticles. The conducting electrons undergo intra-band qualitative excitation above the Fermi energetic levels, based on which the conducting band of a metallic nanoparticle is determined, when photon energy of UV lighting with the highest absorption wavelengths (max) is applied. The possible interaction amid the conducting electrons with the particle's metallic ions is lessened with small particle sizes. As a result, the smaller particle's conduction band energy rises. The Larger particle sizes, on the other hand, include a greater number of atoms, which increases the potential attracting amid conducting electrons and metallic ions and lowers the conducting band energies of metallic nanoparticles [22].

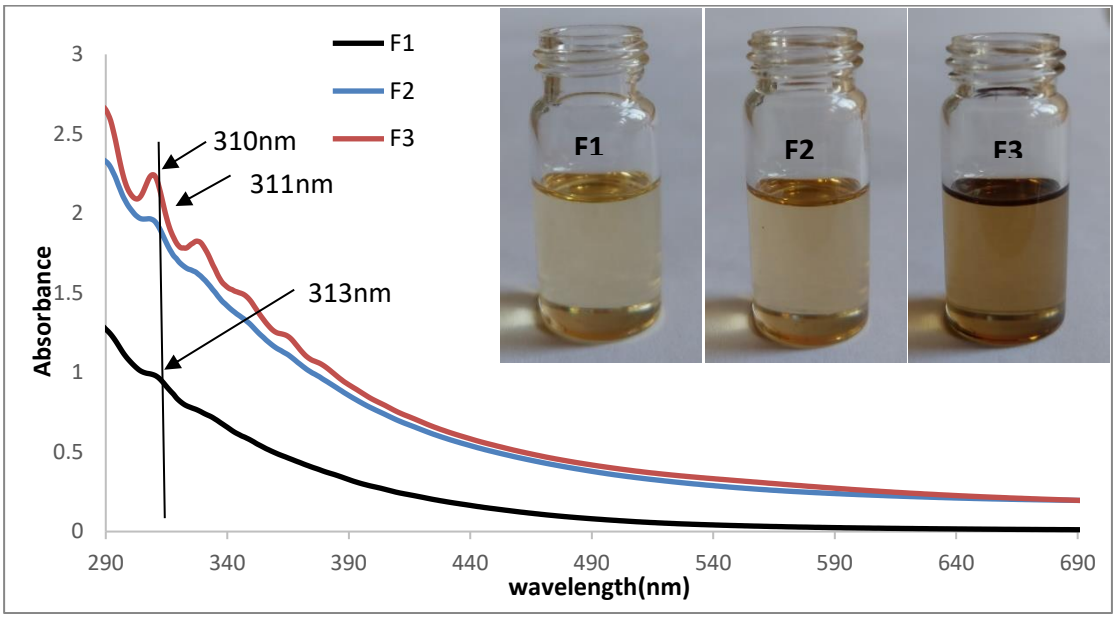

Figure 6a. Optical absorption spectra result of AuQDs Samples in benzene F1, F2 and F3 . The inset photograph Illustration of benzene AuQDs samples.

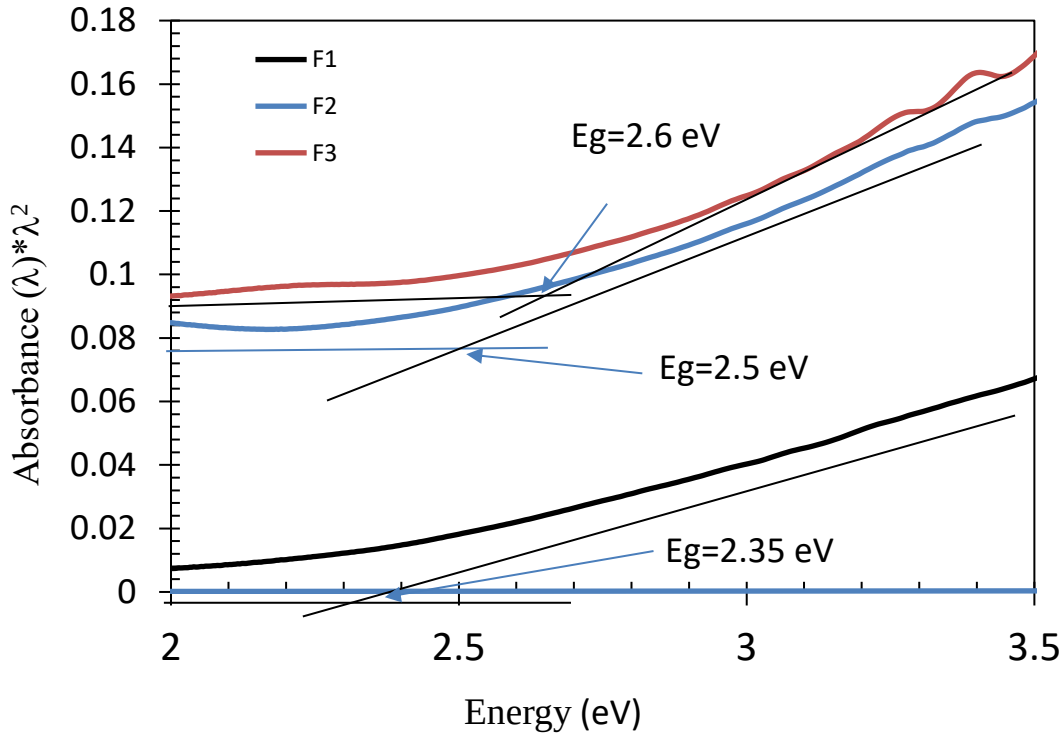

Figure 6b. Energy gaps of the AuQDs samples of F1, F2 and F3, respectively.

The emission spectrums are witnessed with a severe and intensive peak center, as shown in Figure (7a). The Photoluminescence emitting spectra are categorized via the existence of a single severe peak at 481, 445 and 437 nm corresponding to the AuQDs samples F1, F2 and F3, respectively. The emission peaks of AuQDs are due to the electrons' quantum confinements from gold QDs, these peaks were detected at wavelength. The blue shift in the emission peak indicates the smaller QDs [30]. Figure 7 (F1-F2-F3) shows the imaged emission lighting from the AuQDs at the respective energies of 4, 8 and 12 J/cm² (from left to right). However, at higher laser fluence,

the emission seems brighter. The as-created AuQDs had estimated band gaps at 2.58, 2.78, and 2.83 eV, respectively, based on their fluorescent peaks. The QD fluorescing was essentially the radiation of transition from the d to p orbitals, and resulted from molecular-like energy transition amid HOMO-LUMO states [31], where the energy gap agrees with the value obtained from UV-Vis measurements [13]. The blue shift in the fluorescence peak of AuQDs at F3 (12 J/cm^2) was proportional due to the reality that such particles seem to be of small size compared to AuQDs at F1 and F2. Nevertheless, in contrast to the energetic gap amid the energized and ground conditions (the HOMO-LUMO gap) of AuQDs as estimated from the absorbing information (Eg = 2.6 eV), the fluorescence peaks at 437 nm imply a greater comfortable energetic gap (Eg = 2.83 eV) because a charge is transferred from ligands to metals, stabilizing the energetic condition [32], the core's size affects the fluorescent wavelength of AuQDs. The spherical Jellium modelling predicts that small AuQDs radiate at short wavelengths, which implies that raising the quantum sizing causes the fluorescence energy to decrease**.** The blue fluorescent QDs come in a variety of sizes**.** Whereas the larger ones emit at redshift, the smaller ones do so at blue shift. This outcome is in line with the vast size ditrubution of the laser-produced nanoparticles [33].

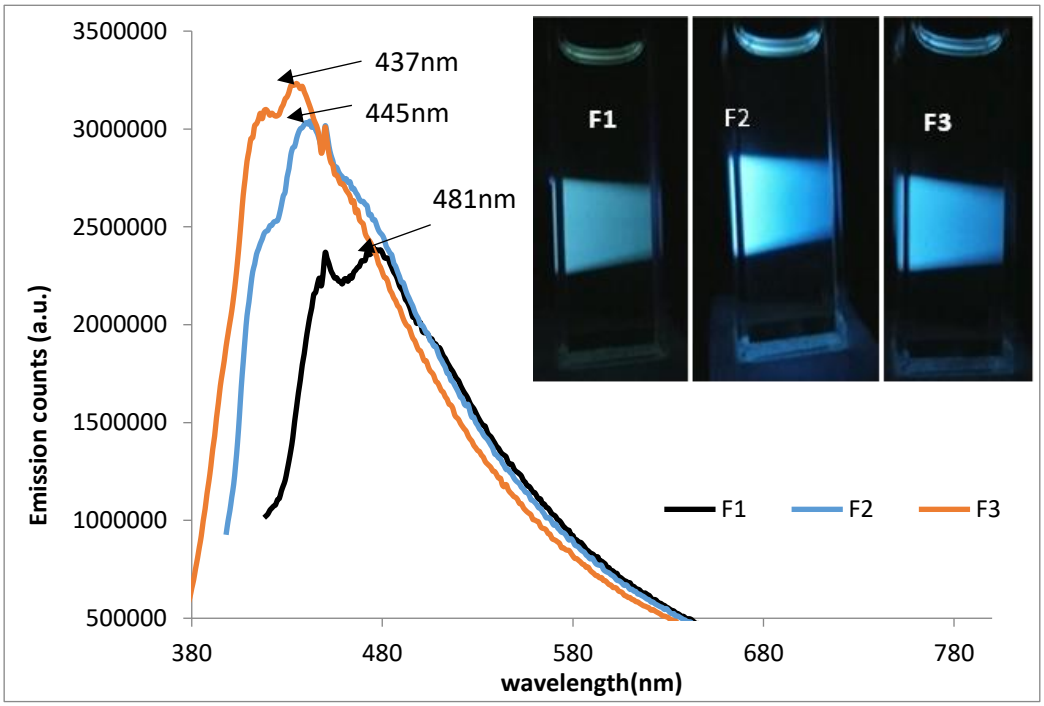

Figure 7. Photoluminescence Emission spectrum of F1, F2 and F3 AuQDs samples. The inset show corresponding emission photographs of pre-prepared samples F1, F2 and F3, respectively.

Figure 8 shows the FTIR spectra result of F3. Various absorbing peaks were found in the FTIR analysis of AuQDs, which helped identify the various functional groups of phytochemicals. The peak 3418cm^{-1} represents the O=H stretch of phenolics, while the 2924 cm^{-1} peak is for C=H stretching of methyl groupings, furthermore 2852 cm^{-1} peak clarifies C=C stretching of alkynes, and the 1652 cm^{-1} peak show C=O stretching of carbonyl groupings of flavonoids and tannins, respectively, were assigned. [30] Also, the peak at 1462, 1260 cm^{-1} represents the C=N stretch of nitriles. The peak 1106 cm^{-1} matches up to the C–O stretch. The peaks observed at 804 correspond to the C–H stretching of alkenes. [34].

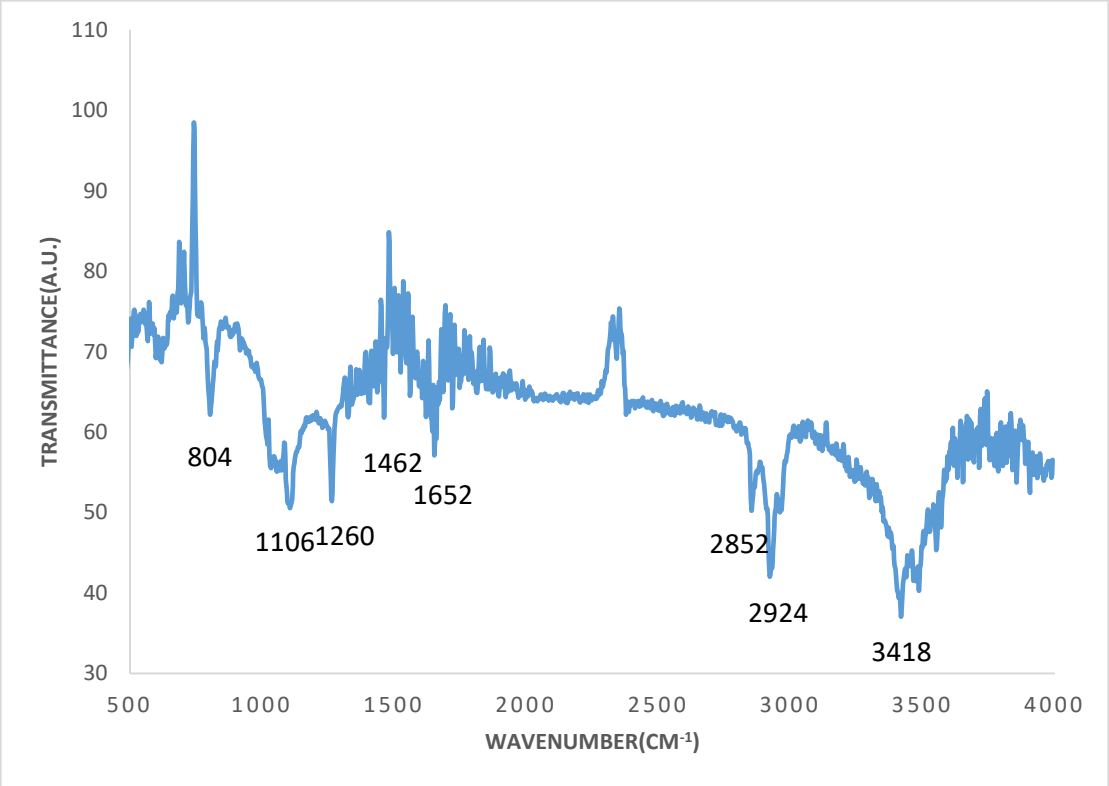

Figure 8. FTIR result for F3 AuQDs sample.

To reveal the chemical structure of the AuQDs, Raman spectra were gathered. Raman scatter has established itself as a key method for learning about the localized structure of various nanoparticles. Due to the great sensitivity of detecting Raman active elements, impurity detection could not be totally disregarded, particularly because the displayed characteristics in the CH stretch area can be challenging to understand. When examining the bonding properties of gold material, Raman spectroscopy is utilized to investigate vibrating, mode systems, and bonding patterns. When a photon from a laser interacts with a molecule's vibrations, it does so through an inelastic lighting scatter process where the molecule might be in a ground or excited condition. The laser-excited AuQDs' molecular vibrating caused the electro-static fields around the metal to become stronger. This technique allowed the AuQDs to exhibit a standard Raman band spanning with a range of 100-3500cm^{-1}. [35]. The outcomes achieved from the Raman spectra of F3 can be seen in Figure 9. The vibrational frequencies exhibited at 2229 cm^{-1} because of C-N stretch vibrations of the compound. According to a previous study [36], the strong bands at 1086 and 1237 cm^{-1} are attributed to C-O stretch vibration. While primary amines exhibit the couple bands of 3209 and 3352 cm^{-1} because of N-H/O-H stretch and symmetrical vibrating, (1791 cm^{-1}) because of C=O stretch, (2581 cm^{-1}) because of CH_3/CH stretch, and at (512-190 cm^{-1}) because of C-H out-of-plane/C-C=O deforming, according to a previous study [35].

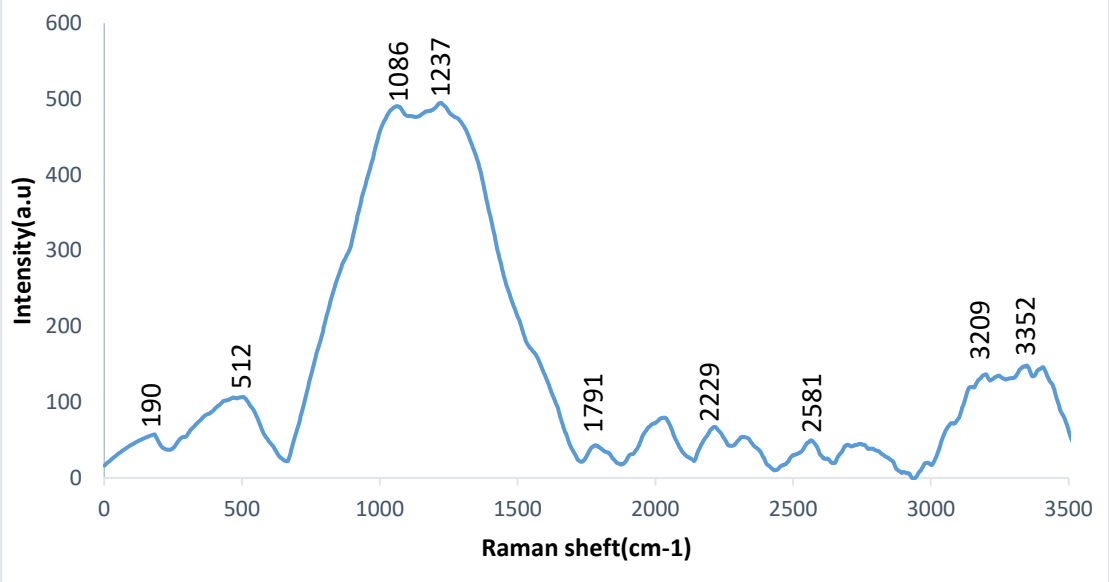

Figure 9. Raman spectra of F3 AuQDs.

5. CONCLUSION

In conclusion, the laser ablating approach has been effectively used to synthesiz AuQDs in benzene solutions, improving production efficacy and reducing particle sizes by studying the effects of laser fluence. As opposed to that, the synthesized AuQDs in benzene solutions have more stability for a long time. Ion-dipoles in benzene prevent AuQDs from forming clumps and preventing agglomeration by interacting with hydroxyl groups (–OH). It was also observed the effect of increasing the energy of the Nd-YAG laser pulse on the particles' size, and the results show that the particles' size decreases when the Energy increases. The results of HR-TEM images and uv-vis analysis show that the band gap increases along with increasing energy, leading to a decrease in the particles' size. The outcomes revealed that the size of the laser-ablated particles decreased as laser intensity increased. When the laser ablating energy was set to 12 J/cm^2, the mean particle size was smaller (less than 5 nm). When the findings are compared to the reference specimen, it is clear that benzene has a substantially faster rate of QDs creation and smaller particle sizes. The ultra-pure and small size produced AuQDs suggest the possibility of using AuQDs in biological applications.

REFERENCES

[1] N. T. Halien, N. D. Hoang, N.T. Nghia, D.Q. Hoa, Synthesis and characterization of fluorescent gold nanoclusters, Vietnam Journal of Chemistry. 56(4) (2018) 460-465.

[2] A.M. Iga, J.H.P. Robertson, M.C. Winslet, A.M. Seifalian, Clinical potential of quantumdots, J. Biomed. Biotechnol. 2007 (2007) 76087.

[3] M.A. Farzin, H. Abdoos, A critical review on quantum dots: From synthesis toward applications in electrochemical biosensors for determination of disease-related biomolecules, talanta. 10 (2020) 121828.

[4] A.R. Ziefuß, S. Reichenberger, C. Rehbock, I. Chakraborty, M. Gharib, W.J. Parak, S. Barcikowski, Laser Fragmentation of Colloidal Gold Nanoparticles with High- Intensity Nanosecond Pulses is Driven by a Single-Step Fragmentation Mechanism with a Defined Educt Particle-Size Threshold, J. Phys. Chem. 122 (2018) 22125–22136

[5] R.L. Calabro, D.S. Yang, D.Y. Kim, Liquid-phase laser ablation synthesis of graphene quantum dots from carbon nano-onions: Comparison with chemical oxidation, J. Colloid Interface Sci. 527 (2018) 132–140.

[6] A.A. Menazea, Femtosecond laser ablation-assisted synthesis of silver nanoparticles in organic and inorganic liquids medium and their antibacterial efficiency, Radiat. Phys.Chem. 168 (2020) 108616.
[7] R. Riedel, N. Mahr, C. Yao, A. Wu, F. Yang, N. Hampp, Synthesis of gold–silica coreshell nanoparticles by pulsed laser ablation in liquid and their physico-chemical properties towards photothermal cancer therapy, Nanoscale 12 (2020) 3007–3018.
[8] R. Das , S. Nath , D. Chakdar , G. Gope, R. Bhattacharjee, Synthesis of silver nanoparticles and their optical Properties, Experimental Nanoscience. 5:4 (2009) 357-362.
[9] T.Higaki, C. Liu, C. Zeng, R. Jin, Y.Chen, N. Rosi, and R Jin, Jin, Controlling the atomic structure of Au30 nanoclusters by a ligandbased strategy, .Angew Chem Int Ed 55 (2016) 6694–6697.
[10] M. Fumitaka, J. Kohono, Y. Takeda, T. Kondow, H.Sawabe, Formation and Size Control of Silver Nanoparticles by Laser Ablation in Aqueous Solution, J. Phys. Chem. B 104, 8333 (2000).
[11] R. A. Ismail, S. Erten-Ela, A. K. Ali, Cagdas Yavuz & K. I. Hassoon, Pulsed Laser Ablation of Tin Oxide Nanoparticles in Liquid for Optoelectronic Devices, Silicon 13 (2021) 3229–3237
[12] R.A. Ismai, M. H. Mohsin, A. K. Ali, K. I. Hassoon, S. Erten-Ela, Preparation and characterization of carbon nanotubes by pulsed laser ablation in water for optoelectronic application, Physica E 119 (2020) 113997.
[13] A. K. Ali, S. Erten-Ela, R. A. Ismail, C. Yavuz, Preparation of blue luminescence gold quantum dots using laser ablation in aromatic solvents, Appl Nanosci 11, (2021) 2779–2791

[14] K. Saware, B. Sawle, B.Salimath, K. Jayanthi, V. Abbaraju, Biosynthesis and characterization of silver nanoparticles using Ficus Benghalensis leaf extract, Engineering and Technology. 2319-1163 (2014) 2321-7308.

[15] M. Abdollahnia , A. MakhdoumiID , M. Mashreghi, H.Eshghi ,Exploring the potentials of halophilic prokaryotes from a solar saltern for synthesizing nanoparticles: The case of silver and selenium, PloS one. 15(3) (2020) e0229886.

[16] K. Maximova, A. Aristov, M. Sentis and A.Kabashin ,Size-controllable synthesis of bare gold nanoparticles by femtosecond laser fragmentation in water ,Nanotechnology. 26 (2015) 065601.

[17] Z. Paranga , A. Keshavarzb, S. Farahi c, S.M. Elahi a, M. Ghorannevissa, S. Parhoodehd "Fluorescence emission spectra of silver and silver/cobalt nanoparticles, Scientia Iranica. 19(3) (2012) 943–947.

[18] C. Li, K.L. Shuford, Q.H. Park, W. Cai, Y. Li, E.J. Lee, S.O. Cho, Highyield synthesis of single-crystalline gold nano-octahedra, Angew Chem. 119 (2007) 3328–3332.

[19] S. Chen, R.Ingram, M. Hostetler, J. Pietron, R. Murray, T. Schaaff, J. Khoury, M. Alvarez, R. Whetten, Gold nanoelectrodes of varied size: transition to molecule-like, charging Science. 280 (1998) 2098–2101.

[20] M. Bracamonte, S. Bollo, P. Labbe, G.A. Rivas, N.F. ferreyra, Quaternized, chitosan as support for the assembly of gold nanoparticles and glucose oxidase. Physiochemical characterization of the platform and evaluation of its biocatalytic activity, Electrochmica Acta 56 (2011) 1316–1322.

[21] C. Chen, Dan Zhao, Y. Jiang, P. Ni, C. Zhang, B. Wang, F.Yang, Y.Lu, J.Sun ,Logically regulating peroxidase-like activity of gold nanoclusters for sensing phosphate-containing metabolites and alkaline phosphatase activity, Anal Chem .91 (2019) 15017–15024.

[22] H. Deng, X. Shi , F. Wang, H. Peng, A. Liu, X. Xia, W. Chen, Fabrication of water-soluble, green-emitting gold nanoclusters with a 65% photoluminescence quantum yield via hostguest recognition, Chem Mater. 29 (2017) 1362–1369.

[23] P. Barone, F. Stranges, M. Barberio,D. Renzelli,A. Bonanno,and F. Xu, Study of band gap of silver nanoparticles Titanium dioxide nanocomposites, J. Chem. 6 (2014) 589707.

[24] Fojtik, A. Henglein, Ber. Busenges., Formation of Nanometer-Size Silicon Particles in a Laser Induced Plasma in SiH4, Phys. Chem. 97 (1993) 252.

[25] D. Kim, S. Jeong, J. Moon, Synthesis of silver nanoparticles using polyol process and the influence of precursor injection, Nanotechnology. 17 (2006) 4019–4024.

[26] Y. Krutyakov, A. Kudrinskiy, A. Olenin, G. Lisichkin, Synthesis and properties of silver nanoparticle: advances and prospects, Russian Chemical. 77 (3) (2008) 233- 257.

[27] K. Brown, D. Walter, M. Natan, Seeding of Colloidal Au Nanoparticle Solutions. 2.Improved Control of Particle Size and Shape, Chem. Mater. 12 (2000) 306–313.

[28] C. Burda, X. Chen, R. Narayanan,M.A. El-Sayed, Chemistry and Properties of Nanocrystals of Different Shapes, Chem. Rev. 105 (2005) 1025-1102.

[29] E. Ali, K .Rasool, W. Abad, A. Abd "Green Synthesis, Characterization and Antimicrobial activity of CuO nanoparticles (NPs) Derived from Hibiscus sabdariffa a plant and CuCl", Conference Series. 1963 (2021) 012092.

[30] A.Keshari , R. Srivastava , P.Singh , V. Yadav , G. Nath ,Antioxidant and antibacterial activity of silver nanoparticles synthesized by Cestrum nocturnum, Ayurveda and Integrative Medicine. xxx (2018) 1-8.

[31] K.Wang, W. Su,F. Gao, X. Gao,W. Niu, H. Yao,X. Wang, and L.Zhao, Glutathione-coated Au29(SG)27: structural determination based on different combination styles confirmed by experiments, J Phys Chem. 123 (2019) 13951–13957.

[32] K. Maximova, A. Aristov, M. Sentis, A.V. Kabashin, Size-controllable synthesis of bare gold nanoparticles by femtosecond laser fragmentation in water, Nanotechnology. 26 (2015) 065601.

[33] P. Šmejkal, J. Pfleger, B. Vlˇcková ,Study of laser fragmentation process of silver nanoparticles in aqueous media, Appl Phys. 93 (2008) 973–976.

[34] R. velana, P. Ayyasamya , R. Kathiravanb , B. Subashni, Rapid decolorization of synthetic melanoidin by bacterial extract and their mediated silver nanoparticles as support, Journal of Applied Biology & Biotechnology. 3 (02) (2015) 006-011.

[35] T. Devi, S. Gayathri, FTIR AND FT-RAMAN SPECTRAL ANALYSIS OF PACLITAXEL DRUGS, Pharmaceutical Sciences. 2 (2010) 0976 – 044.

[36] M. Bindhu, M. Umadevi, Silver and gold nanoparticles for sensor and antibacterial applications, Molecular and Biomolecular Spectroscopy. 128 (2014) 37–45.